AKAP95 organizes a nuclear microdomain to control local cAMP for regulating nuclear PKA

Terri Clister[1,2], Eric C. Greenwald[2], George S. Baillie[3], Jin Zhang*[1,2]

[1]Department of Pharmacology and Molecular Sciences, Johns Hopkins University School of Medicine, Baltimore, MD 21205, USA [2]Department of Pharmacology, University of California, La Jolla, CA 92093, USA [3]Department of Molecular Pharmacology, Institute of Cardiovascular and Medical Science, College of Medical, Veterinary and Life Sciences, University of Glasgow, Glasgow G12 8QQ, Scotland, UK

*Corresponding Author and Lead Contact

Correspondence: Jin Zhang, 9500 Gilman Drive, BRF-II 1120, La Jolla, CA 92093-0702, phone (858) 246-0602, email jzhang32@ucsd.edu

Summary

Contrary to the classic model of PKA residing outside of the nucleus, we identify a nuclear signaling complex that consists of AKAP95, PKA, and PDE4D5 and show that it forms a functional cAMP signaling microdomain. Locally generated cAMP can accumulate within the vicinity of this complex; but when cAMP is generated at the plasma membrane, PDE4 serves as a local sink and PDE3 as a barrier to prevent accumulation of cAMP within the microdomain as a means of controlling activation of tethered nuclear PKA.

Keywords: *imaging, FRET biosensors, compartmentalization, spatiotemporal*

Introduction

Protein kinase A (PKA) is a ubiquitous serine/threonine kinase involved in regulating multiple cellular processes. The PKA holoenzyme is a tetramer composed of a specific regulatory subunit isoform (RIα, RIβ, RIIα, or RIIβ) homodimer and two catalytic subunits, where each catalytic subunit is bound to a regulatory subunit in the dimer. Activation of PKA occurs when cAMP binds the regulatory subunits, unleashing the active catalytic subunits. In the classic understanding of the pathway, PKA signaling in the nucleus was thought to occur by activation of extranuclear PKA and diffusion of the catalytic subunit into the nucleus. Recent studies raise some questions as to whether or not the catalytic subunit of the PKA holoenzyme completely dissociates under physiological conditions (Smith et al., 2013, 2017). In the absence of translocated catalytic subunit, nuclear PKA signaling would need to be activated and regulated through alternative mechanisms. Our previous work suggests that a pool of activatable PKA holoenzyme exists in the nucleus, which can be activated by local cAMP generated in the cytosol or nucleus (Sample et al., 2012). Consistent with our findings, a recent study showed that high cAMP production resulting from synergistic actions of two GPCRs at the endosome can lead to the activation of nuclear PKA (Jean-Alphonse et al., 2016). However, the molecular components that localize this pool of PKA to the nucleus and the mechanism by which nuclear PKA is controlled locally remain to be identified.

AKAP95, a PKA RII binding protein, has been shown to localize to the nucleus. It has been associated with multiple functions, including chromatin condensation, RNA processing, and gene expression, and recently its upregulation has been correlated with increased cyclin D1 and E1 expression in multiple types of cancer (Akileswaran et al., 2001; Arsenijevic et al., 2004, 2006; Coghlan et al., 1994; Collas et al., 1999; Eide et al., 2002, 2003; Jiang et al., 2013;

Marstad et al., 2016; Zhao et al., 2015). We hypothesized that AKAP95 is a nuclear AKAP that anchors a specific pool of PKA holoenzyme within the nucleus.

Results

AKAP95 forms an endogenous complex with PKA and PDE

To determine if AKAP95 forms a complex with PKA holoenzyme in the nucleus, we isolated nuclear proteins from HEK293T cells. These nuclear lysates endogenously contain AKAP95 (Figure 1a). The western blot results were further supported by immunofluorescence studies that detected AKAP95 in the nucleus (Figure 1b).

To better characterize AKAP95 in the nucleus we performed fluorescence recovery after photobleaching (FRAP) experiments using GFP-tagged AKAP95. On average, bleached areas showed a half recovery time of 25.7 ± 5.7 s (Supplemental Figure 1a) (N=11 cells). Based on these experiments, the majority of AKAP95 is mobile in the nucleus, with an average mobile fraction of 65.8 ± 11.2%. Interestingly, the observed AKAP95 puncta do not easily recover after photobleaching (Supplemental Figure 1b and 1c), suggesting that AKAP95 within these puncta is less mobile.

In addition to AKAP95, endogenous RIIα and the catalytic subunit of the PKA holoenzyme (PKAcat) were also detected in the nucleus with nuclear fractionation followed by western blotting (Figure 1a) as well as immunofluorescence (Figure 1b). For RIIα and PKAcat, the nuclear staining is significantly less than the cytosolic staining, but is clearly above background (Supplemental Figure 1d, e). Previous studies suggest PDEs, specifically PDE4D isoforms, are directly involved in regulating nuclear PKA activity (Sample et al., 2012). We

found evidence of PDE4D, specifically isoform PDE4D5, in the nucleus (Figure 1a) where PDE4D5 appears to form puncta (Figure 1b).

To determine if the different components can form a complex in the nucleus, co-immunoprecipitation studies on the nuclear lysates were performed. We first pulled down endogenous AKAP95 and found that it associates with endogenous PKA RIIα, PKAcat, and PDE4D5 (Figure 2a), which was further confirmed via reciprocal co-immunoprecipitation experiments in which we isolated RIIα or PDE4D5 and probed for the remaining components (Figure 2a). The signals were detected above the background from normal IgG controls, indicating the specificity of these interactions.

Further support for the endogenous nuclear AKAP95 complex containing PKA and PDE4D comes from proximity ligation assay (PLA) experiments. In these experiments complexes containing AKAP95 and RIIα were detected in intact, fixed cells (Figure 2b). On average 1.65 ± 0.17 dots per nuclei (N=66 cells) were observed when measuring the AKAP95 and RIIα interaction, which is significantly ($p<0.0001$) above the background signal observed with AKAP95 (Figure 2b) or RIIα (Supplementary Figure 1f-g) antibody alone (0.40 ± 0.09 dots/nuclei, N=53 cells). Interestingly, although by immunofluorescence AKAP95 and RIIα are mainly detected in the nucleus and cytoplasm, respectively, PLA signal was observed in both the nucleus and cytoplasm (Supplemental Figure 1f-g). Therefore, although there are limited amounts of AKAP95 and RIIα in specific subcellular compartments, they are still interacting in a significant way. PDE4D5 and AKAP95 were also observed to interact in the PLA experiments with an average of 3.80 ± 0.33 dots per nuclei (N=79 cells), which is significantly above the background signal produced by AKAP95 antibody alone ($p<0.0001$). These results suggest that AKAP95 forms a complex with a resident pool of nuclear PKA, as well as PDE4D5.

The AKAP95 microdomain tightly regulates cAMP

The identification of AKAP95 as a specific nuclear scaffold protein that binds to PKA and PDE allows us to directly test the hypothesis that PDEs co-anchored to the same AKAP complex help regulate the activation of this PKA pool by reducing local cAMP levels. First, we employed our previously developed mathematical model (Sample et al., 2012) to generate predictions of the localized cAMP dynamics within the nuclear AKAP compartment. This ordinary differential equation model was developed to test hypotheses for differences in cAMP dynamics between the cytosol and nucleus. We extended the model to include a FRET-based cAMP biosensor, ICUE3 (DiPilato and Zhang, 2009), in the nuclear AKAP compartment and used the previously developed parameters and initial conditions to predict how cAMP dynamics will differ between the general nucleus and AKAP95 compartments (Figure 3a, b). This model predicts that when a modest amount of cAMP is generated at the plasma membrane, the nucleus experiences increased cAMP accumulation, but the nuclear AKAP compartment does not. Furthermore, the model predicts that higher cAMP production can overcome PDE-mediated inhibition in the AKAP compartment, such that cAMP accumulates in both the general nucleus and nuclear AKAP compartments.

To test these predictions experimentally, we targeted the FRET-based cAMP biosensor ICUE3 to AKAP95 to measure cAMP levels around AKAP95. This biosensor contains a cAMP binding domain sandwiched between a FRET pair and reports cAMP dynamics via changes in FRET. Targeting of this biosensor to AKAP95 was achieved using a chemically induced dimerization approach based on FK506 binding protein (FKBP) and FKBP-rapamycin binding domain (FRB), two proteins that bind specifically and tightly in the presence of rapamycin

(Banaszynski et al., 2005). This chemically inducible targeting system was chosen to avoid concerns of expressing a large fusion protein in the nuclear compartment. Although not utilized here, this system could offer some flexibility for experimental designs to evaluate nuclear and AKAP95 compartments in the same cells before and after rapamycin. FKBP was fused to the N-terminus of nuclear-localized ICUE3 (FKBP-ICUE3-NLS), and FRB was fused to the C-terminus of human AKAP95 (AKAP95-FRB) (Figure 3c and Supplemental Figure 2a). When HEK293T cells co-expressing FKBP-ICUE3-NLS and AKAP95-FRB were treated with rapamycin (100 nM), the diffuse pattern of reporter fluorescence became more punctate within the nucleus within minutes, indicating the translocation and recruitment of ICUE3 to AKAP95 (Supplemental Figure 2b). HEK293T cells co-expressing these same two constructs were treated with rapamycin or DMSO (control) and harvested for co-immunoprecipitation experiments. Immunoprecipitation using anti-AKAP95 antibody followed by western blotting for GFP revealed that ICUE3 interacted with AKAP95 in cells treated with rapamycin, confirming the localization of the reporter to AKAP95 (Supplemental Figure 4c). To ensure that targeting ICUE3-NLS to AKAP95 did not affect the dynamic range of the reporter, the maximum responses of cells expressing either FKBP-ICUE3-NLS alone (N=39 cells) or both FKBP-ICUE3-NLS and AKAP95-FRB (N=35 cells) were compared (Supplemental Figure 4d). In both cases, cells were treated with rapamycin, and the maximum response was stimulated by the addition of forskolin and IBMX to activate adenylyl cyclases and inhibit PDEs, respectively. After rapamycin treatment, the biosensor responded similarly to maximal cAMP stimulation regardless of AKAP95-FRB co-expression, indicating that the dynamic range of the biosensor is not affected by its localization to AKAP95.

To determine what effect the site of cAMP generation has on the cAMP levels within the AKAP95 compartment, we combined live-cell imaging using the localized cAMP biosensor with spatiotemporal manipulation of cAMP using soluble adenylyl cyclase (sAC), or SMICUS, which is a method previously developed to generate local pools of cAMP using subcellularly targeted sAC (Sample et al., 2012). sAC is pharmacologically distinct from the transmembrane adenylyl cyclase (tmAC). Instead of being activated by GPCRs, it is activated by bicarbonate, ATP, or calcium (Zippin et al., 2013). We can therefore use exogenously expressed mCherry-tagged sAC as a tool to generate cAMP in specific subcellular locations in a dose-dependent manner in HEK293T cells by the addition of sodium bicarbonate to the culture medium (Sample et al., 2012). To this end, mCherry-tagged sAC was localized to either the plasma membrane (PM-sAC) or the nucleus (sAC-NLS) (Figure 3c). PM-sAC generates cAMP at the plasma membrane, mimicking the production of cAMP by tmACs. HEK293T cells expressing PM-sAC and either FKBP-ICUE3-NLS alone for general nuclear targeting, or FKBP-ICUE3-NLS plus AKAP95-FRB for AKAP95 targeting, were first treated with rapamycin (100 nM) (Figure 3d). Cells were then treated with a low dose (2.5 mM) of sodium bicarbonate to activate targeted sAC. Although cAMP production at the plasma membrane by sub-maximal sAC activation led to a clear response in the general nuclear compartment within 15 min, with an average emission ratio change of 11.3 ± 1.5% (N=39 cells), cAMP was not detected within the AKAP95 microdomain (mean emission ratio change -1.9 ± 0.8%, N=35 cells), suggesting that cAMP accumulation is tightly regulated in the area surrounding the AKAP95 complex, which represents a functional microdomain with distinct cAMP dynamics. Subsequent treatment with a saturating dose (15 mM) of bicarbonate to maximally activate sAC resulted in increased FRET responses from both nuclear-localized and AKAP95-targeted ICUE3 (Figure 3d). Hence, although some cAMP

158 generated at the plasma membrane is able to diffuse into the nucleus, an added level of
159 regulation limits the accumulation of cAMP within the AKAP95 microdomain. While there are
160 differences in kinetics, these data qualitatively agree with the model predictions of an ablated
161 cAMP response to the low stimulation condition in the AKAP95 compartment but a response to
162 the high stimulation condition.

163 Next, the cAMP responses within the AKAP95 compartment were compared when
164 cAMP was generated at the plasma membrane or within the nucleus. When cAMP was generated
165 in the nuclei of cells expressing sAC-NLS, even a low dose of sodium bicarbonate resulted in
166 clear cAMP responses of 4.9 ± 0.8% within the AKAP95 microdomain (N=18 cells) compared to
167 the lack of a response within the microdomain when cAMP was generated at the plasma
168 membrane (-0.9 ± 0.8%, N=18 cells) (Figure 3e). Maximal activation of sAC in the nucleus or at
169 the plasma membrane further increased the cAMP levels in the AKAP95 microdomain.

170 These findings further support the existence of a functional microdomain that is distinct
171 from the general nuclear environment in the immediate vicinity of AKAP95, where cAMP
172 accumulation is limited unless cAMP is generated more locally or in excess levels from the
173 plasma membrane. These results support the hypothesis that AKAP95 is able to create a distinct
174 microdomain that limits cAMP concentrations, thereby providing a way to tune the activation
175 threshold of the AKAP-anchored pool of PKA.

176

177 <u>PDE4 and PDE3 have distinct roles in regulating cAMP around AKAP95</u>

178 To test the role of different PDE classes in regulating the microdomain, we used
179 inhibitors specific to either PDE4 or PDE3. HEK293T cells expressing PM-sAC and rapamycin-
180 induced AKAP95-targeted ICUE3 were treated with rolipram (PDE4 inhibitor), milrinone

(PDE3 inhibitor) or vehicle control. Cells were subsequently treated with a low dose (2.5 mM), followed by a high dose (15 mM), of sodium bicarbonate to activate PM-sAC.

The initial response after the addition of PDE inhibitor indicates the basal level of PDE activity at the microdomain. As shown in Figure 4a and b, cells treated with the PDE4 inhibitor rolipram (1 μM) exhibited an immediate increase in cAMP levels in the AKAP95 microdomain (9.4 ± 1.9% emission ratio change, N=29 cells), suggesting that co-anchored PDE4 is basally active in restricting cAMP levels within the AKAP95 microdomain. Subsequent addition of low-dose sodium bicarbonate following PDE4 inhibition further increased cAMP levels in the microdomain (10.0 ± 0.8%, N=29 cells), in sharp contrast to the limited response (4.9 ± 0.8%, N=39 cells) in the absence of any inhibitor (Figure 4c). Furthermore, a dominant-negative mutant of PDE4D5 (dnPDE4D5) was used as an alternative to global PDE4 inhibition by rolipram to more specifically investigate the role of PDE4D isoforms at the microdomain. This dominant-negative mutant is inactive and does not directly inhibit endogenous PDEs, but instead competes with and displaces them from binding to scaffolding proteins such as AKAP95 (Terrin et al., 2006). We can therefore specifically interrogate the role of the scaffolded PDE4D5 in regulating the AKAP95 microdomain. HEK293T cells expressing AKAP95-targeted ICUE3, PM-sAC, and a dominant-negative mutant of PDE4D5 were treated with a low dose followed by a high dose of sodium bicarbonate. Cells expressing the mutant PDE4D5 exhibited a robust cAMP response to submaximal activation of PM-sAC (16.5 ± 1.9%, N=24 cells) compared with control cells that were not transfected with dominant-negative PDE4D5 (-1.9 ± 0.8%, N=35 cells) (Figure 4d). These data suggest that basally active PDE4 restricts cAMP accumulation in the AKAP95 microdomain under both basal state and stimulated conditions.

In contrast, addition of the PDE3 inhibitor milrinone (10 μM) induced no response within the microdomain (2.0 ± 1.3%, N=19 cells) (Figure 4a-b), suggesting PDE3 does not play a role in controlling the basal level of cAMP within the AKAP95 microdomain. Interestingly, when PDE3 is inhibited with milrinone, submaximal activation of PM-sAC led to increased cAMP levels in the microdomain (13.4 ± 1.8%, N=19 cells) (Figure 4c), indicating that PDE3 plays a role in preventing low levels of plasma membrane-generated cAMP from accessing the microdomain.

Discussion

Here we presented the identification of a nuclear signaling complex consisting of AKAP95, PKA, and PDE4D5. AKAP95 has previously been found to bind RIIα during mitosis after the nuclear envelope has dissolved (Collas et al., 1999). Using both nuclear fractionation studies and whole-cell immunofluorescence experiments we demonstrate that nuclear AKAP95 interacts with the regulatory subunit of PKA during interphase. These findings suggest that AKAP95 can anchor PKA in the nucleus irrespective of cell cycle stages. Previous studies have found that AKAP95 can associate with PDE4A in T-lymphocytes, but the functional role of anchored PDE4A was not tested (Asirvatham et al., 2004). Here we show that anchored PDE4D5 plays a critical role in the functional cAMP signaling microdomain assembled by AKAP95.

The roles played by different PDE isoforms are complex. Although it is widely accepted that cAMP diffusion is controlled and limited, the mechanisms underlying this compartmentalization are debated. One model for cAMP regulation suggests the existence of a barrier to prevent cAMP diffusion away from a particular location (e.g., the plasma membrane).

225 An alternative model posits that PDEs concentrate in certain locations to prevent cAMP
226 accumulation at those locations. Our results suggest these two mechanisms could co-exist in a
227 PDE isoform-specific manner. PDE4 isoforms are part of a complex with AKAP95 and create a
228 local sink to limit the accumulation of cAMP within the AKAP95 microdomain. Our data
229 suggest that PDE3 is not a part of the AKAP95 complex but could act as a gate to prevent free
230 diffusion of cAMP from the plasma membrane, the specific mechanisms and functional roles of
231 which will be further investigated. The intricate interplay between these two different PDE
232 isoforms and their effects on local signaling expands the concept of localized cAMP
233 compartmentalization control to include proximate and distal PDE isoforms working in concert.
234 cAMP is thus tightly regulated within this microdomain to prevent accidental nuclear PKA
235 activation and reserve this pool of scaffolded PKA holoenzyme for transducing signals that
236 generate specific, local sources of cAMP.

237 What are the specific signals that can lead to the activation of this pool of nuclear PKA
238 holoenzymes? Endogenous sAC has been shown to localize to subcellular locations such as the
239 cytosol, nucleus, and mitochondria and respond to changes in bicarbonate, calcium, and ATP.
240 sAC has been shown to act as a sensor for changes in pH and metabolism in different cell types
241 (Tresguerres et al., 2010, 2011, Zippin et al., 2003, 2010, 2013) and could generate cAMP
242 proximal to this pool of nuclear PKA. In addition, it has been demonstrated that endocytosed
243 GPCRs continue signaling at the endosome and that this endosomal signaling elicits distinct
244 transcriptional responses (Irannejad et al., 2013; Tsvetanova and von Zastrow, 2014). cAMP
245 generated at the endosome could provide a local source of cAMP that activates the nuclear PKA
246 pool. Supporting this hypothesis, Jean-Alphonse et al (Jean-Alphonse et al., 2016) recently
247 showed that a synergistic effect between PTHR and β_2-AR signaling induces pronounced

endosomal cAMP production that corresponds with activation of nuclear PKA and increased levels of phosphorylated CREB, a PKA substrate. Given that GPCR internalization and endosomal cAMP production vary by receptor and ligand, the strength and extent of nuclear PKA activation by internalized GPCRs may be receptor specific. The tight regulation of cAMP, and by extension nuclear PKA, within the AKAP95 microdomain shown here provides a new example of signaling specificity arising from precise spatiotemporal control.

Significance

PKA signaling is integral to numerous cellular processes, and the spatiotemporal control of PKA is necessary for the regulation of its diverse downstream effects. The discovery and characterization of a nuclear PKA signaling microdomain further complicates the classical understanding of PKA signaling. Instead of PKA activation occurring only in the cytosol, these findings suggest there exists a distinct nuclear pool of PKA that is reserved for sensing more "proximal" signals because the AKAP95 assembled nuclear microdomain specifically allows accumulation of locally generated cAMP. This study also demonstrates a clear example of synergistic effects of isoform-specific PDEs, where PDE4 is responsible for creating a local cAMP sink but also relies on more distal PDE3 to act as a gate and prevent the free diffusion of cAMP from overwhelming the local PDE4. The studies discussed in this article expand our understanding of PKA signaling and regulation. Furthermore, the knowledge gained by understanding the regulation of nuclear PKA, a prototypic kinase and signaling molecule, can aid in developing better models for the study of spatiotemporal regulation of other signaling molecules.

Acknowledgements

We would like to thank J. Scott for the AKAP95 cDNA and T. Inoue for the FKBP/FRB cDNA. We thank L. Joosen for technical help with confocal and FRAP imaging. We thank S. Mehta for aid in preparing figures and text. This work was funded by R01 DK073368 (to J. Z.) and F32 GM120798-02 (to E.G.).

Author Contribution

TC and JZ conceived all experiments. EG designed and performed modeling analysis. TC performed all other experiments. GSB provided critical reagents and advice. TC and JZ wrote the manuscript.

Competing financial interests

The authors declare no competing financial interests.

References

Akileswaran, L., Taraska, J.W., Sayer, J.A., Gettemy, J.M., and Coghlan, V.M. (2001). A-kinase-anchoring Protein AKAP95 Is Targeted to the Nuclear Matrix and Associates with p68 RNA Helicase. J. Biol. Chem. *276*, 17448–17454.

Arsenijevic, T., Degraef, C., Dumont, J.E., Roger, P.P., and Pirson, I. (2004). A novel partner for D-type cyclins: protein kinase A-anchoring protein AKAP95. Biochem. J. *378*, 673–679.

Arsenijevic, T., Degraef, C., Dumont, J.E., Roger, P.P., and Pirson, I. (2006). G1/S cyclins interact with regulatory subunit of PKA via A-kinase anchoring protein, AKAP95. Cell Cycle *5*, 1217–1222.

Asirvatham, A.L., Galligan, S.G., Schillace, R. V., Davey, M.P., Vasta, V., Beavo, J.A., and Carr, D.W. (2004). A-Kinase Anchoring Proteins Interact with Phosphodiesterases in T

Lymphocyte Cell Lines. J. Immunol.

Banaszynski, L.A., Liu, C.W., and Wandless, T.J. (2005). Characterization of the FKBP-rapamycin-FRB ternary complex. J. Am. Chem. Soc. *127*, 4715–4721.

Coghlan, V.M., Langeberg, L.K., Fernandez, A., Lamb, N.J.C., and Scott, J.D. (1994). Cloning and characterization of AKAP 95, a nuclear protein that associates with the regulatory subunit of type II cAMP-dependent protein kinase. J. Biol. Chem.

Collas, P., Le Guellec, K., and Taskén, K. (1999). The A-kinase-anchoring protein AKAP95 is a multivalent protein with a key role in chromatin condensation at mitosis. J. Cell Biol. *147*, 1167–1179.

DiPilato, L.M., and Zhang, J. (2009). The role of membrane microdomains in shaping beta2-adrenergic receptor-mediated cAMP dynamics. Mol. Biosyst. *5*, 832–837.

Eide, T., Carlson, C., Taskén, K.A., Hirano, T., Taskén, K., and Collas, P. (2002). Distinct but overlapping domains of AKAP95 are implicated in chromosome condensation and condensin targeting. EMBO Rep. *3*, 426–432.

Eide, T., Taskén, K.A., Carlson, C., Williams, G., Jahnsen, T., Taskén, K., and Collas, P. (2003). Protein kinase A-anchoring protein AKAP95 interacts with MCM2, a regulator of DNA replication. J. Biol. Chem. *278*, 26750–26756.

Irannejad, R., Tomshine, J.C., Tomshine, J.R., Chevalier, M., Mahoney, J.P., Steyaert, J., Rasmussen, S.G.F., Sunahara, R.K., El-Samad, H., Huang, B., et al. (2013). Conformational biosensors reveal GPCR signalling from endosomes. Nature *495*, 534–538.

Jean-Alphonse, F.G., Wehbi, V.L., Chen, J., Noda, M., Taboas, J.M., Xiao, K., and Vilardaga, J.-

P. (2016). β2-adrenergic receptor control of endosomal PTH receptor signaling via Gβγ. Nat. Chem. Biol. *13*, 259–261.

Jiang, H., Lu, X., Shimada, M., Dou, Y., Tang, Z., and Roeder, R.G. (2013). Regulation of transcription by the MLL2 complex and MLL complex-associated AKAP95. Nat. Struct. Mol. Biol. *20*, 1156–1163.

Marstad, A., Landsverk, O.J.B., Strømme, O., Otterlei, M., Collas, P., Sundan, A., and Brede, G. (2016). A-kinase anchoring protein AKAP95 is a novel regulator of ribosomal RNA synthesis. FEBS J. *283*, 757–770.

Sample, V., DiPilato, L.M., Yang, J.H., Ni, Q., Saucerman, J.J., and Zhang, J. (2012). Regulation of nuclear PKA revealed by spatiotemporal manipulation of cyclic AMP. Nat. Chem. Biol. *8*, 375–382.

Smith, F.D., Reichow, S.L., Esseltine, J.L., Shi, D., Langeberg, L.K., Scott, J.D., and Gonen, T. (2013). Intrinsic disorder within an AKAP-protein kinase A complex guides local substrate phosphorylation. Elife *2*.

Smith, F.D., Esseltine, J.L., Nygren, P.J., Veesler, D., Byrne, D.P., Vonderach, M., Strashnov, I., Eyers, C.E., Eyers, P.A., Langeberg, L.K., et al. (2017). Local protein kinase A action proceeds through intact holoenzymes. Science (80-.). *356*, 1288–1293.

Terrin, A., Di Benedetto, G., Pertegato, V., Cheung, Y.F., Baillie, G., Lynch, M.J., Elvassore, N., Prinz, A., Herberg, F.W., Houslay, M.D., et al. (2006). PGE1 stimulation of HEK293 cells generates multiple contiguous domains with different [cAMP]: Role of compartmentalized phosphodiesterases. J. Cell Biol. *175*, 441–451.

Tresguerres, M., Parks, S.K., Salazar, E., Levin, L.R., Goss, G.G., and Buck, J. (2010). Bicarbonate-sensing soluble adenylyl cyclase is an essential sensor for acid/base homeostasis. Proc. Natl. Acad. Sci. U. S. A. *107*, 442–447.

Tresguerres, M., Levin, L.R., and Buck, J. (2011). Intracellular cAMP signaling by soluble adenylyl cyclase. Kidney Int. *79*, 1277–1288.

Tsvetanova, N.G., and von Zastrow, M. (2014). Spatial encoding of cyclic AMP signaling specificity by GPCR endocytosis. Nat. Chem. Biol. *10*, 1061–1065.

Zhao, S., Yi, M., Yuan, Y., Zhuang, W., Zhang, D., Yu, X., Chen, X., Teng, B., Guan, Z., and Zhang, Y. (2015). Expression of AKAP95, Cx43, CyclinE1 and CyclinD1 in esophageal cancer and their association with the clinical and pathological parameters. Int. J. Clin. Exp. Med. *8*, 7324–7332.

Zippin, J.H., Chen, Y., Nahirney, P., Kamenetsky, M., Wuttke, M.S., Fischman, D.A., Levin, L.R., and Buck, J. (2003). Compartmentalization of bicarbonate-sensitive adenylyl cyclase in distinct signaling microdomains. FASEB J. *17*, 82–84.

Zippin, J.H., Chadwick, P.A., Levin, L.R., Buck, J., and Magro, C.M. (2010). Soluble adenylyl cyclase defines a nuclear cAMP microdomain in keratinocyte hyperproliferative skin diseases. J. Invest. Dermatol. *130*, 1279–1287.

Zippin, J.H., Chen, Y., Straub, S.G., Hess, K.C., Diaz, A., Lee, D., Tso, P., Holz, G.G., Sharp, G.W.G., Levin, L.R., et al. (2013). CO2/HCO3-- and calcium-regulated soluble adenylyl cyclase as a physiological ATP sensor. J. Biol. Chem. *288*, 33283–33291.

Main figure titles and legends

Figure 1: AKAP95, PKA, and PDE are present in the nucleus

a) Western blot images of whole-cell, non-nuclear, and nuclear HEK293T lysates reveal localization of AKAP95, PKARIIα, and PKAcat within the nucleus. PDE4D5 is also detected in nuclear fractions, though PDE3B is not. β-tubulin antibody staining shows a lack of cytosolic protein in the nuclear fraction, and probing for CREB provides a positive control for nuclear isolation. b) Representative images showing immunofluorescence staining of endogenous protein similarly detects the candidate proteins in the nucleus. Scale bars, 10 μm (See Supplemental Figure 1 for quantification of nuclear localization of PKAcat and PKA RIIα).

Figure 2: AKAP95 forms an endogenous complex with PKA and PDE

a) Co-immunoprecipitation of nuclear fractions of HEK293T cells show interactions between AKAP95, RIIα and PDE4D5. The left column shows the AKAP95 IP, including lanes for the nuclear lysate input, AKAP95 IP, and the control IP using normal IgG. PDE4D5 (indicated by arrow), RIIα, and PKAcat are detected in the AKAP95 pulldown. The other components are also detected in immunprecipitates of RIIα or PDE4D5, shown in the right columns (western blot images representative of 2 or 3 repeated experiments). b) Proximity Ligation Assay (PLA) was performed with AKAP95 (N = 53 cells) and either RIIα (N = 66 cells) or PDE4D5 (N = 79 cells). Representative images are shown with quantification of nuclear PLA signal (average ± SEM). *** signifies $p<0.0001$. (See also Supplemental Figure 1). The co-IP and PLA experiments indicate that RIIα, AKAP95, PDE4D5 form a complex within the nucleus of HEK293T cells.

Figure 3: The AKAP95 microdomain tightly regulates cAMP

a) Based on a previous computational model for nuclear PKA activity, a new model was developed to predict cAMP levels in the AKAP microdomain and nucleus when cAMP is

generated at the plasma membrane in a dose-dependent manner using PM-sAC. b) The model suggests different cAMP responses in the nucleus (orange) and AKAP microdomain (black) upon low-dose (LD, 2.5 mM) and high-dose (HD, 15 mM) $NaHCO_3$ stimulation of cAMP production by PM-sAC. c) Using the FKBP/FRB dimerization system to localize ICUE3 to AKAP95, the model predictions were directly tested under three different experimental conditions: cAMP generated by PM-sAC and detected by the cAMP biosensor ICUE3 targeted to either i.) the nucleus or ii.) the AKAP95 microdomain of HEK293T cells, or iii.) cAMP generated in the nucleus by sAC-NLS and detected by AKAP95-targeted ICUE3. (See Supplemental Figure 3 for representative images). d) ICUE3 emission ratio (cyan/yellow) responses in the nucleus (orange, N=39 cells) and in the AKAP95 microdomain (black, N=35 cells) stimulated by LD $NaHCO_3$ (2.5 mM) followed by HD (15 mM) in HEK293T cells expressing PM-sAC. Shown is the average trace ± SEM. Comparison of the maximum responses to LD $NaHCO_3$ shows a significant difference between the microdomain and nucleus ($p<0.0001$). e) ICUE3 emission ratio (cyan/yellow) responses in the AKAP95 microdomain stimulated by LD $NaHCO_3$ (2.5 mM) followed by HD (15 mM) in HEK293T cells expressing PM-sAC (black, N=18 cells) or sAC-NLS (red, N=18 cells). The maximum response to LD $NaHCO_3$ in the microdomain when cAMP is generated at the plasma membrane is significantly different compared with cAMP generated in the nucleus (inset, $p<0.0001$).

Figure 4: PDE4 and PDE3 have distinct roles in regulating cAMP around AKAP95

The effect of isoform-specific PDE inhibition was tested in the AKAP95 microdomain. Cells expressing AKAP95-targeted ICUE3 and PM-sAC were co-treated with PDE inhibitor and rapamycin (100 nM) and subsequently with $NaHCO_3$ (LD, 2.5 mM; HD, 15 mM) to generate cAMP at the plasma membrane via PM-sAC. a) AKAP95-targeted ICUE3 emission ratio

401 (cyan/yellow) responses when cells were treated with the PDE4 inhibitor rolipram (1 μM)
402 (purple, N=29 cells), the PDE3 inhibitor milrinone (10 μM) (blue, N=19 cells), or without
403 inhibitor treatment (black, N=39 cells). Cells were additionally treated with a low dose (LD, 2.5
404 mM) and subsequently a high dose (HD, 15 mM) of $NaHCO_3$. b) The initial FRET response after
405 inhibitor addition indicates basal PDE activity in the AKAP95 microdomain. The change in
406 normalized ICUE3 emission ratio (cyan/yellow) is shown. There is a statistically significant
407 response in cells treated with rolipram ($p<0.0001$) but not in cells treated with milrinone
408 ($p=0.1293$). c) After low-dose $NaHCO_3$ stimulation, a statistically significant response is
409 observed in PDE4-inhibited cells ($p<0.0001$) and PDE3-inhibited cells ($p=0.0002$) compared to
410 cells lacking inhibitor treatment. d) AKAP95-targeted ICUE3 emission ratio (cyan/yellow)
411 responses in cells expressing dnPDE4D5 (purple, N=24 cells) or cells not expressing dominant
412 negative PDE isoforms (black, N=35 cells). Cells were treated with LD (2.5 mM) followed by
413 HD (15 mM) $NaHCO_3$ to stimulate PM-sAC. e) LD PM-sAC stimulation induced statistically
414 significant responses in cells expressing the dominant negative PDE4D5 compared to control
415 cells (inset, $p<0.0001$).

416

417 **Methods**

418 **CONTACT FOR REAGENT AND RESOURCE SHARING**

419 Further information and requests for resources and reagents should be directed to and will be
420 fulfilled by the Lead Contact, Jin Zhang (jzhang32@ucsd.edu).

421 **EXPERIMENTAL MODEL AND SUBJECT DETAILS**

422 **Cell Culture**

HEK293T cells (human embryonic kidney, female) were maintained in DMEM (10% (v/v) FBS and 1% (v/v) penicillin-streptomycin at 37°C with 5% CO_2.

METHOD DETAIL

Nuclear Fractionation

Sucrose-gradient centrifugation was used to isolate and collect nuclei. All steps were performed on ice. HEK293T cells were collected in DPBS and pelleted at 470 × g for 10 min. Gentle vortexing was used to resuspend the cell pellet in ice-cold Sucrose Buffer I (0.32 M), and cells were lysed by 15 strokes of a Dounce homogenizer B pestle. Lysates were gently mixed with Sucrose Buffer II (2.0 M) in a 50 mL tube. The lysate-sucrose mix was layered on top of Sucrose Buffer II in a polyallomer SW 40.1 ultracentrifuge tube. Any space remaining in the tube was filled with Sucrose Buffer I. A Beckman centrifuge with a SW41 Ti rotor was used to separate the nuclei at 30,000 rpm for 45 min, at 4°C. Whole-cell, non-nuclear, and nuclear fractions were probed with antibodies against CREB (Cell Signaling 9197S) and β-tubulin (Cell Signaling 2146S) to ensure clean fractionation. Antibodies used on fractionation samples: AKAP95 (R-146) (Santa Cruz, sc-10766), RIIα (H-12) (Santa Cruz, sc-137220), PKAcat (A-2) (Santa Cruz, sc-28315), PDE3B (H-300) (Santa Cruz, sc-20793), and PDE4D5 (gift from Dr. George Baillie).

Co-Immunoprecipitation

Protein A/G PLUS-Agarose beads (Santa Cruz sc-2003) or Protein A/G Magnetic Beads (bimake.com B23202) were equilibrated in Tris buffer. Pre-clearing was achieved by incubation of agarose beads with 1 mg of nuclear protein and 5 μg rabbit IgG (Santa Cruz sc-2027) for 1 h at 4°C to remove proteins that nonspecifically bind the beads or IgG. Pre-cleared lysate was

incubated with the immunoprecipitating antibody for 1 h at 4°C. The lysate-antibody mix was incubated with agarose beads overnight. After 4 washes with ice-cold DPBS, bound protein was eluted by boiling for 5 min in SDS sample buffer. Antibodies used for Co-IP: PKA IIα reg (C-20) (sc-908), PDE4D5 (gift from Dr. George Baillie's Lab), AKAP95 (R-146) (sc-10766), Clean Blot (Thermo Fisher Scientific 21230).

Immunofluorescence Imaging

Cells were rinsed in HBSS and then fixed in 4% PFA for 30 min, followed by permeabilization for 1 h at room temperature. Cells were then incubated overnight at 4°C or for 30 min at 37°C with primary antibody. Alexa Fluor 488-conjugated and Alexa Fluor 568-conjugated secondary antibodies (Thermo Fisher Scientific A-11034, A-11001, A-11011, or A-11004) were incubated at room temperature for 1 h or 30 min at 37°C in the dark. Cells were incubated with Hoescht 33342 stain at room temperature for 30 min before imaging. Cells were imaged on a Zeiss LSM 880 Confocal with Airyscan processing using a 40x/1.2NA objective. Images were acquired with the suggested settings using 405 nm, 488 nm, and 561 nm lasers. Antibodies used for IF: AKAP95 (F-11) (Santa Cruz, sc-390335) or AKAP95 (R-146) (Santa Cruz, sc-10766), RIIα (C-20) (Santa Cruz, sc-908), PKAcat (BDBiosciences Clone 5B cat#610980), PDE4D3 (gift from Dr. George Baillie), and PDE4D5 (gift from Dr. George Baillie).

Proximity Ligation Assay

PLA experiments were performed using the Duolink® in situ red starter kit for proximity ligation assays (Sigma Aldrich, DUO92101) according to the provided protocol. The only protocol modification was to extend the amplification time by 50 min. Briefly, cells were fixed and permeabilized as in the immunofluorescence experiments before incubation with primary

antibody (same used for IF experiments), then with the provided secondary antibody (conjugated with nucleotides) for 30 min at 37°C each with washes after each step. Ligation of the nucleotides and amplification of the strand occurred sequentially by incubating cells with first ligase then polymerase and detection solution. PLA experiments with AKAP95 antibodies from different species were used as positive controls, and experiments with just one primary antibody (AKAP95) provided our negative control. Images were acquired on a Zeiss LSM 880 Airyscan confocal as described above. A cross section of the nucleus (3.6-5 μm) was acquired and the number of dots within that cross section counted both inside and outside the nucleus.

Computational Modeling

A previously developed computational model of compartmentalized cAMP and PKA dynamics in HEK293 cells (Sample et al., 2012) was modified to include ICUE in the nuclear AKAP compartment and evaluated in MATLAB (Mathworks). Briefly, the "nucAKAP Model" is a compartmental ordinary differential equation (ODE) model that consists of plasma membrane, cytosol, nucleus and nuclear AKAP compartments. This model consists of equations describing cAMP production by adenylyl cyclases (both endogenous and over-expressed sAC), cAMP degradation by PDEs, and cAMP activation of PKA. Additionally, the cAMP biosensor ICUE and PKA biosensor AKAR were included in all the compartments except for the nuclear AKAP compartment. We extended this "nucAKAP Model" to include ICUE in the nuclear AKAP compartment by making the following modifications.

A new second-order reaction of cAMP binding to ICUE in the nuclear AKAP compartment:

$$\frac{dICUEc_{AKAP}}{dt} = k_{f,ICUE} \cdot cAMP_{AKAP} \cdot ICUE_{AKAP} - k_{r,ICUE} \cdot ICUEc_{AKAP}$$

And an additional conservation of mass equation for total ICUE in the nuclear AKAP compartment:

$$ICUE_{AKAP} = ICUEtot_{AKAP} - ICUEc_{AKAP}$$

And finally, the conservation of mass for free cAMP in the nuclear AKAP compartment was updated to account for the cAMP that is bound to ICUE.

$$cAMP_{AKAP} = cAMPtot_{AKAP} - RaC_{AKAP} - RbC_{AKAP} - 2RabC_{AKAP} - Ra_{AKAP} - Rb_{AKAP} - 2Rab_{AKAP} - ICUEc_{AKAP}$$

No new kinetic parameters were introduced, as the rates of cAMP association and dissociation with ICUE are assumed to be consistent across compartments. Total ICUE in the AKAP compartment, $ICUEtot_{AKAP}$, was assumed to be equal to the total amount of PKA in the AKAP compartment, which assumes that each AKAP has both PKA and ICUE bound to it. All other equations and parameters are as described in the supplement of Sample et al 2012 (Sample et al., 2012).

This model was run using the initial conditions from the published model and allowed to equilibrate by running for 10^9 s. Using the simulated plasma membrane-targeted sAC built into the model ($E_{sAC,pm,basal} = 1.663 \cdot 10^{-1}$ mM/s), cAMP production was stimulated with a low dose of $NaHCO_3$ (increase $E_{sAC,pm,basal}$ by $1x1.726 \cdot 10^{-1}$) for 15 min and then subjected to a high dose of $NaHCO_3$ (increase $E_{sAC,pm,basal}$ by $6x1.726 \cdot 10^{-1}$) for another 15 min.

Cloning

Full-length human AKAP95 was kindly provided by Dr. John D. Scott (University of Washington). FKBP and FRB constructs were kindly provided by Dr. Takanari Inoue (Johns Hopkins University). FRB or GFP were tagged to the C-terminus of AKAP95 using BamHI and EcoRI or NotI restriction sites. FKBP with a flexible linker was added to the N-terminus of ICUE3 (DiPilato and Zhang, 2009) using HindIII and BamHI restriction sites.

Live-cell Imaging

HEK293T cells were transfected with Lipofectamine 2000 (Invitrogen) when cells were 50-60% confluent and imaged 16-24 h later. Cells were washed twice with and maintained in Hank's balanced salt solution buffer (HBSS). Cells were imaged at room temperature.

FRAP Imaging

FRAP experiments were performed on a Leica TCS SP8 confocal microscope using its associated FRAP software, a 63x/1.4NA objective, and a DD488/552 beamsplitter. A total of 5 images were acquired before bleaching a rectangular cross-section or circular area of the nucleus with 25% laser power. Post-bleaching images were acquired every 5 or 10 s for at least 5 min. Images were analyzed using the Jython script found at: http://imagej.net/Analyze_FRAP_movies_with_a_Jython_script.

FRET Imaging

Prior to imaging, cells were equilibrated in HBSS for 10 min in a CO_2-independent incubator. Cells were treated with $NaHCO_3$ (J.T. Baker, purity=100%), which induced a small change in FRET for the FKBP-tagged biosensor with or without co-expression of AKAP95-FRB (seen in Figure 3), forskolin (Calbiochem, purity ≥99% by HPLC), IBMX (Sigma, purity ≥98% by TLC), rolipram (Alexis, purity ≥98% by TLC), or milrinone (Alexis, purity ≥97% by TLC) as

indicated. Cells were imaged on a Zeiss Axio Observer Z1 microscope equipped with a 40x/1.3 NA objective and Photometrics Evolve 512 EMCCD, using METAFLUOR 7.7 software (Molecular Devices) to control dual-emission-ratio imaging acquisition every 30 s. A 420DF20 excitation filter, a 450DRLP dichroic mirror, and two emission filters (475DF40 for CFP and 535DF25 for YFP) alternated by a Lambda 10-2 filter-changer (Sutter instruments) were used for the FRET measurements. The microscope settings for RFP (sAC) fluorescence acquisition were as follows: 555DF25 excitation filter, 568rdc dichroic mirror, and 650DF100 emission filter. Exposure times for all channels ranged from 50-500 ms. Emission intensities of individual cells were background-subtracted, and the ratio between the CFP and FRET channel was normalized to the timepoint just before addition of low-dose $NaHCO_3$ (t = 0 min). Because overexpressed sAC has some basal activity prior to stimulation, the starting FRET ratio for AKAP95-localized ICUE3 was higher in cells expressing sAC-NLS compared to PM-sAC. Therefore, a moderate range of overlap in starting ratios between these two experiments was determined, and cells were selected for comparison based on starting ratio within this range to control for basal activity differences. On the other hand, the expression of PM-sAC was controlled to be within a defined range, and this range was held constant between different experimental conditions; cells outside this range were excluded from analysis.

QUANTIFICATION AND STATISTICAL ANALYSIS

2-3 biological replicates were done for Co-IP and PLA experiments, and at least 3 biological replicates performed for all other experiments. Unpaired two-tailed t-tests with Welch's correction were used for statistical analyses, done in Graphpad Prism. *** indicates a p-

548 value<0.0001. N values, as indicated in figure legends and the main text, represent number of

549 cells. All error bars indicate standard error.

550 **KEY RESOURCES TABLE**

REAGENT or RESOURCE	SOURCE	IDENTIFIER
Antibodies		
Goat anti-mouse Alexa Fluor 488-conjugate	Thermo Fisher Scientific	Cat# A-11001, RRID:AB_2534069
Goat anti-rabbit Alexa Fluor 568-conjugate	Thermo Fisher Scientific	Cat# A-11011, RRID:AB_143157
Goat anti-mouse Alexa Fluor 568-conjugate	Thermo Fisher Scientific	Cat# A-11004, RRID:AB_2534072
Goat anti-rabbit Alexa Fluor 488-conjugate	Thermo Fisher Scientific	Cat# A-11034, RRID:AB_2576217
PKA RIIa (C-20) monoclonal rabbit	Santa Cruz Biotechnology	Cat# sc-908, RRID:AB_632214
PKA RIIa (H-12) monoclonal mouse	Santa Cruz Biotechnology	Cat# sc-137220, RRID:AB_2268608
AKAP95 (R-146) polyclonal rabbit	Santa Cruz Biotechnology	Cat# sc-10766, RRID:AB_2226060
AKAP95 (F-11) monoclonal mouse	Santa Cruz Biotechnology	Cat# sc- 390335
PKAcat (A-2) monoclonal rabbit	Santa Cruz Biotechnology	Cat# sc-28315, RRID:AB_628136
PKAcat (Clone 5B) monoclonal mouse	BD Biosciences	Cat# 610980, RRID:AB_398293
CREB monoclonal rabbit	Cell Signaling Technology	Cat# 9197, RRID:AB_331277
β-Tubulin polyclonal rabbit	Cell Signaling Technology	Cat# 2146, RRID:AB_2210545
PDE3B polyclonal rabbit	Santa Cruz Biotechnology	Cat# sc-20793, RRID:AB_2283579
PDE4D3 rabbit	Dr. George Baillie	n/a
PDE4D5 rabbit	Dr. George Baillie	n/a
Clean Blot	Thermo Fisher Scientific	Cat# 21230
Bacterial and Virus Strains		

E. coli DH5α	Thermo Fisher Scientific	Cat# 18265017
Biological Samples		
Chemicals, Peptides, and Recombinant Proteins		
BamHI	Thermo Fisher Scientific	Cat# FD0054
EcoRI	Thermo Fisher Scientific	Cat# FD0274
NotI	Thermo Fisher Scientific	Cat# FD0594
HindIII	Thermo Fisher Scientific	Cat# FD0504
$NaHCO_3$	J.T. Baker	Cat# 3506-01
forskolin	Calbiochem	Cat# 344270
milrinone	Alexis	Cat# ALX-270-083-M005
IBMX	Sigma	Cat# I5879
rolipram	Alexis	Cat# ALX-270-119
Critical Commercial Assays		
Duolink® in situ red starter kit	Sigma	DUO92101
Deposited Data		
Experimental Models: Cell Lines		
HEK293T	ATCC	CRL-11268
Experimental Models: Organisms/Strains		
Oligonucleotides		
Recombinant DNA		
Full-length human AKAP95	Dr. John D. Scott (University of Washington)	
FRB	Dr. Takanari Inoue (Johns Hopkins University)	
FKBP	Dr. Takanari Inoue (Johns Hopkins University)	
Software and Algorithms		
FRAP Analysis Jython Script	http://imagej.net/Analyze_FRAP_movies_with_a_Jython_script	
ImageJ	NIH	imagej.nih.gov/ij/

MATLAB	Mathworks	https://www.mathworks.com/products/matlab.html
Prism 5	GraphPad Software	www.graphpad.com
METAFLUOR 7.7	Molecular Devices	www.moleculardevices.com
Leica Application Suite, Advanced Fluorescence FRAP wizard	Leica	www.leica-microsystems.com
Other		
Protein A/G Magnetic Beads for IP	Bimake.com	Cat# B23202
Protein A/G PLUS-agarose beads	Santa Cruz Biotechnology	Cat# sc-2003, RRID:AB_10201400

551

Figure1

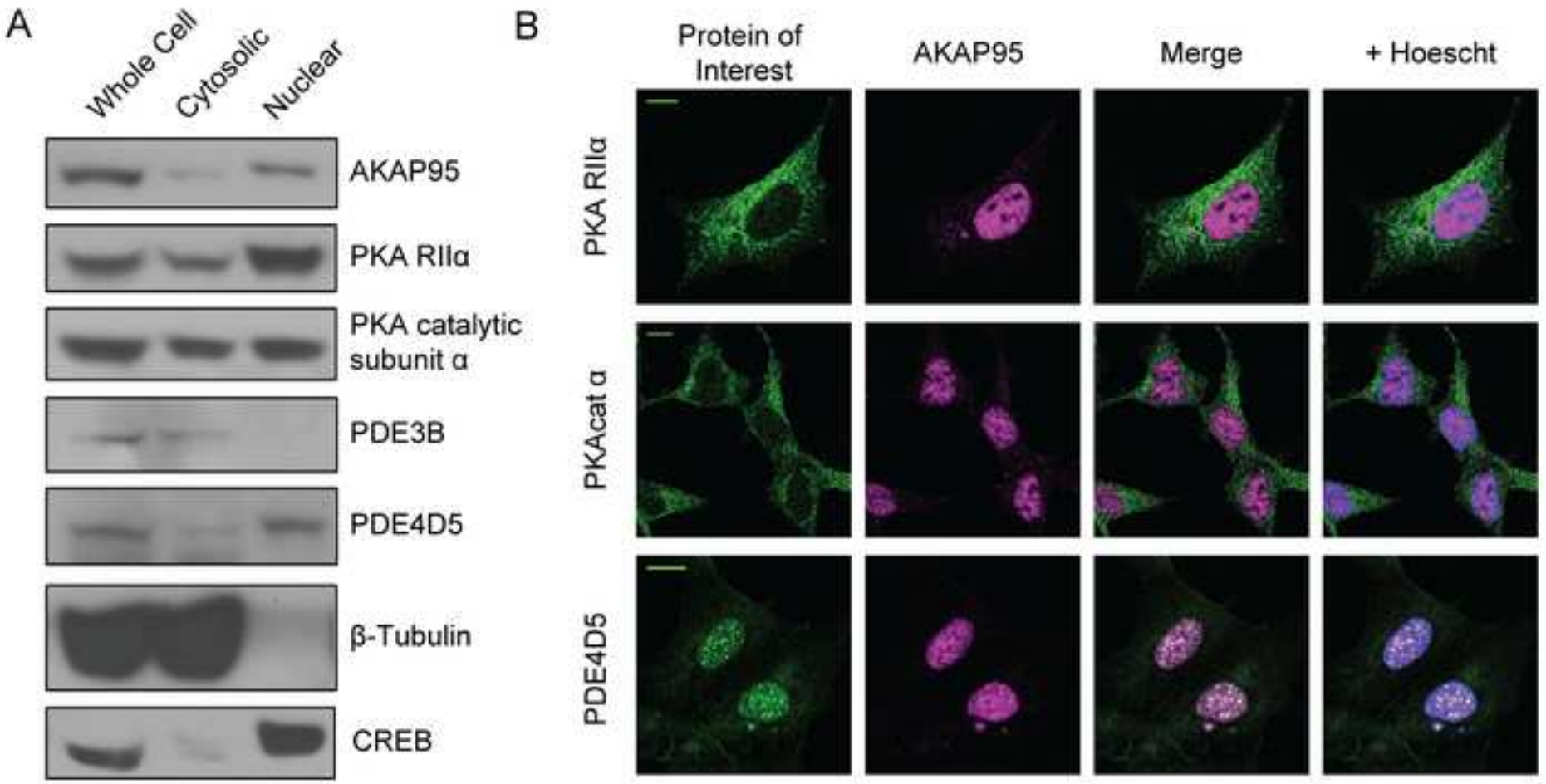

Figure2

Click here to access/download;Figure;Figure2.tif

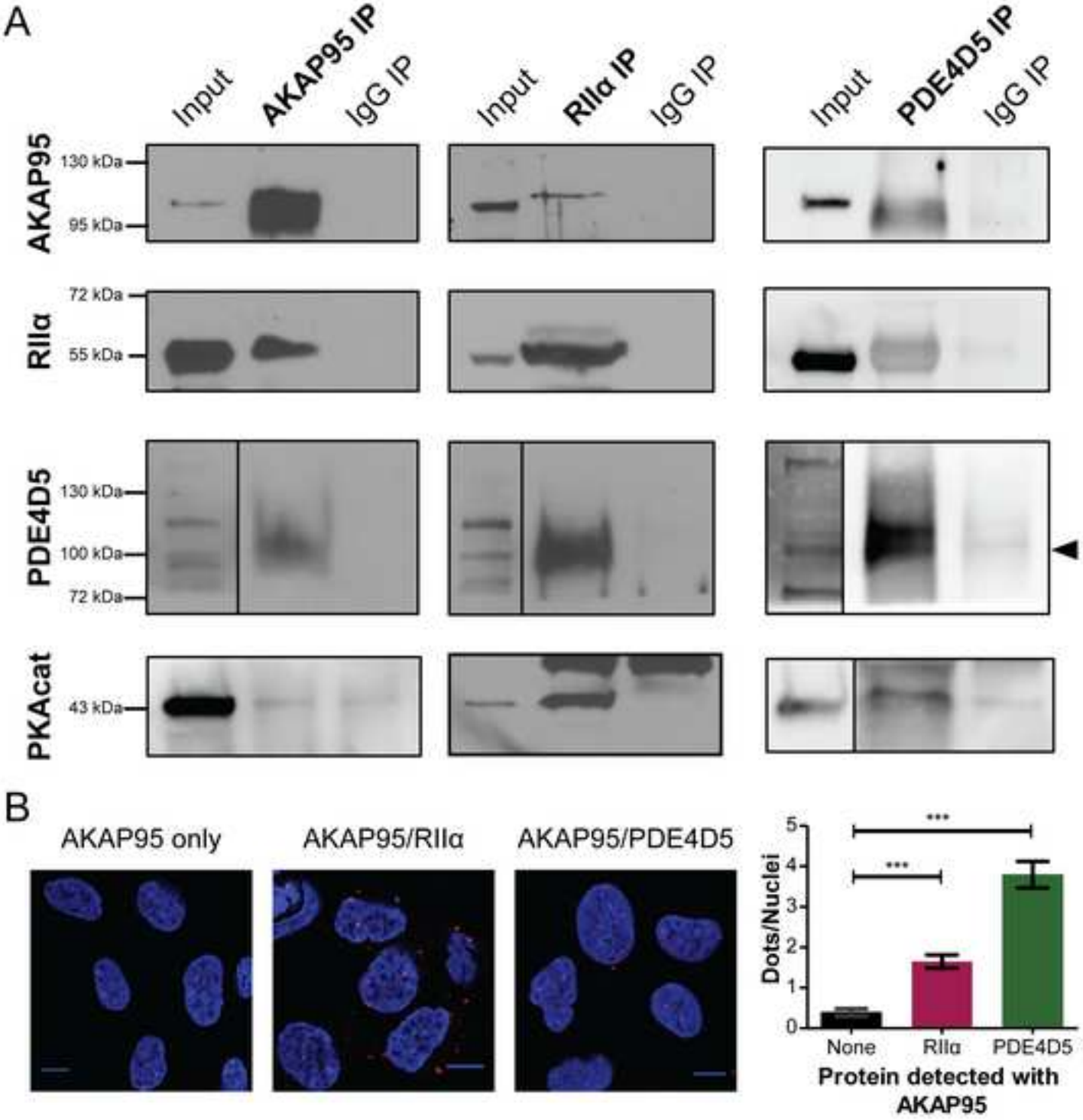

Figure3

Click here to access/download;Figure;Figure3.tif

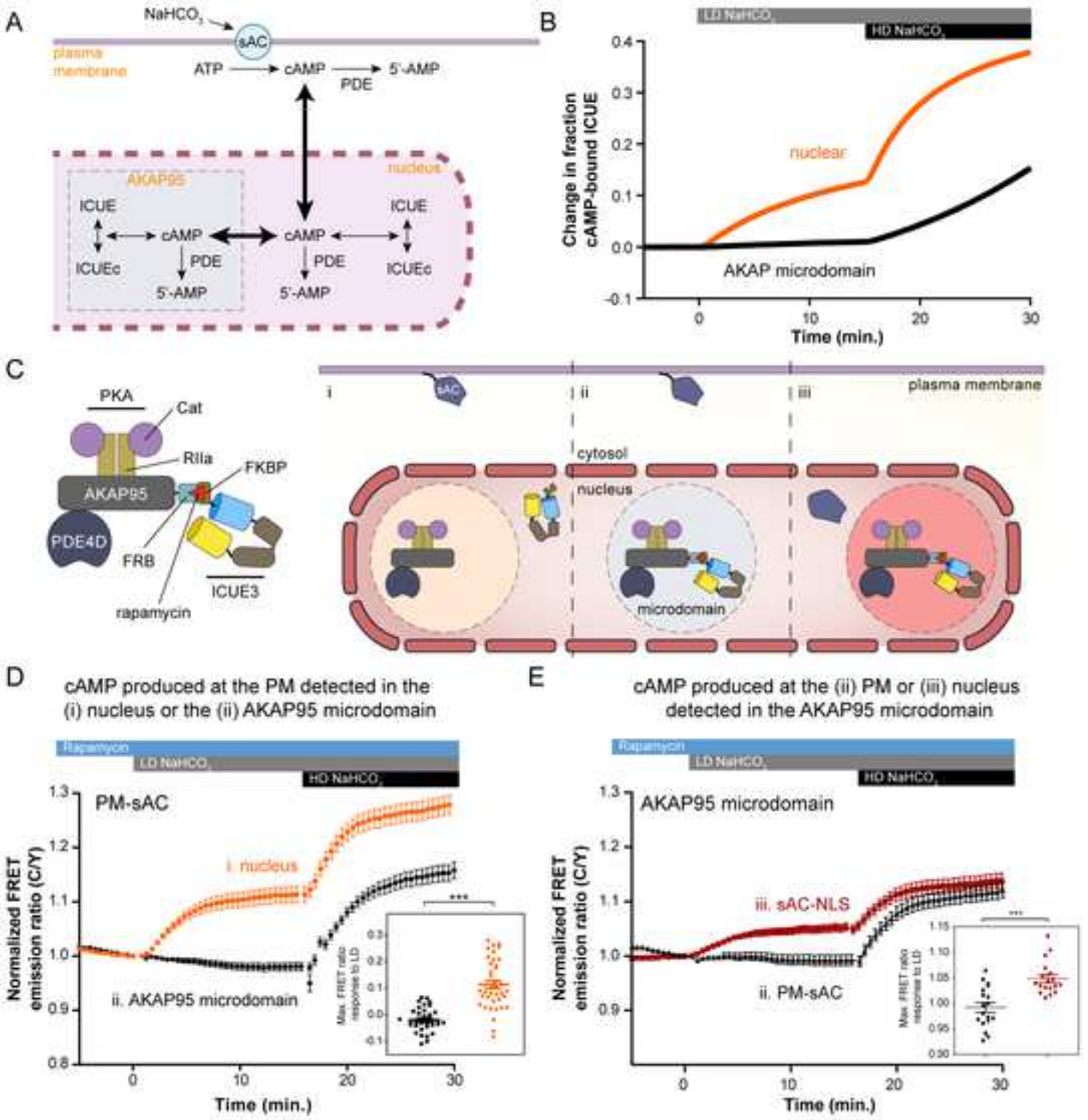

Figure4

Click here to access/download;Figure;Figure4.tif

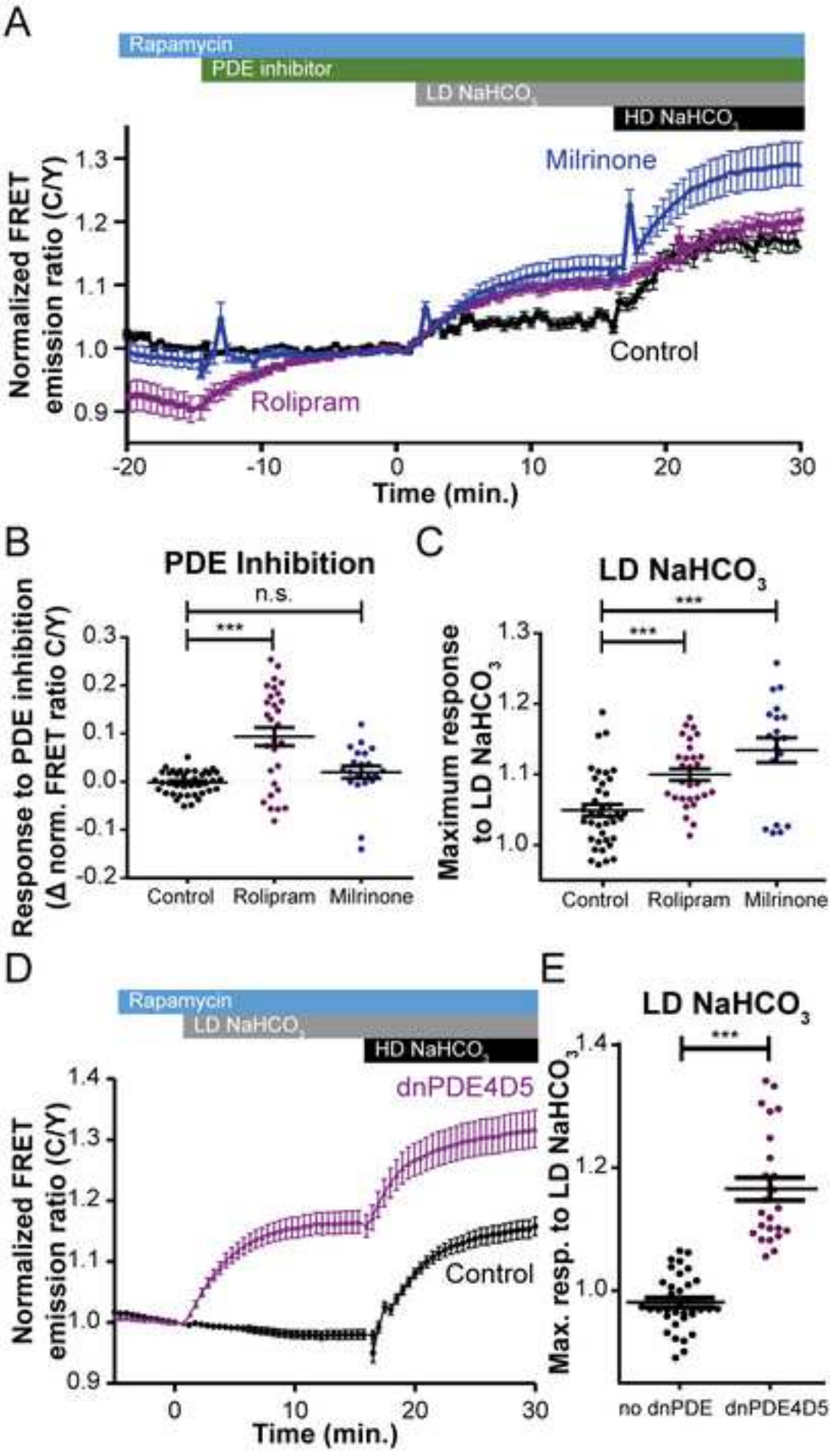

Supplemental Figures

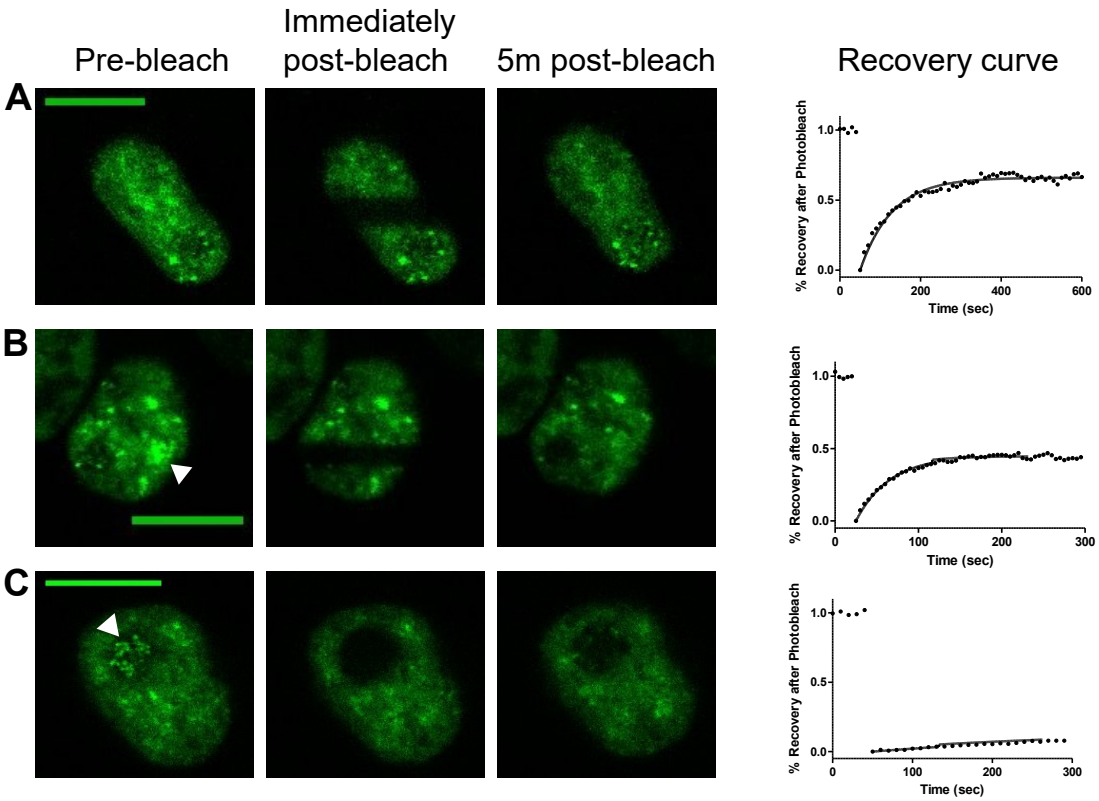

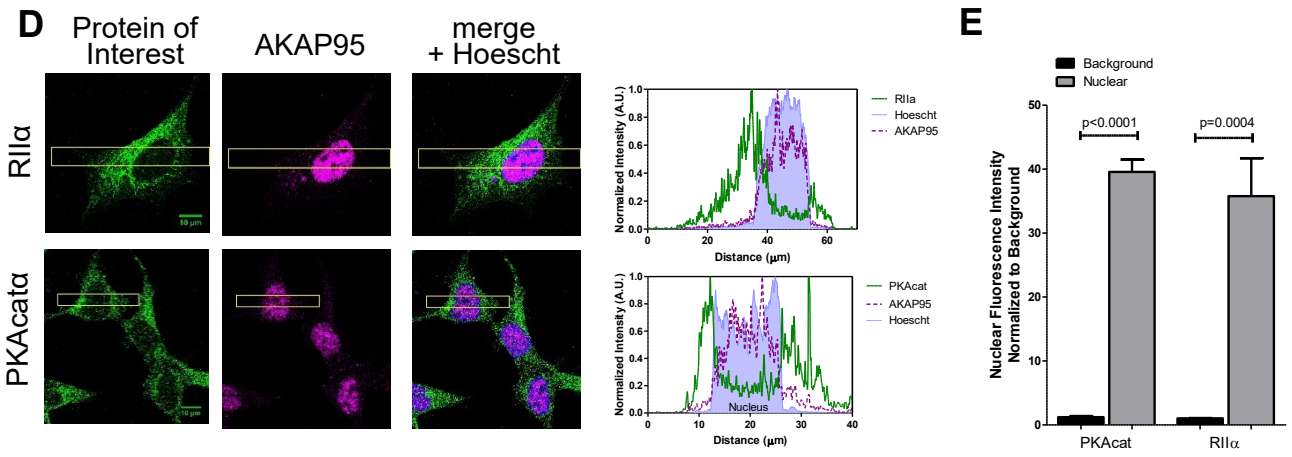

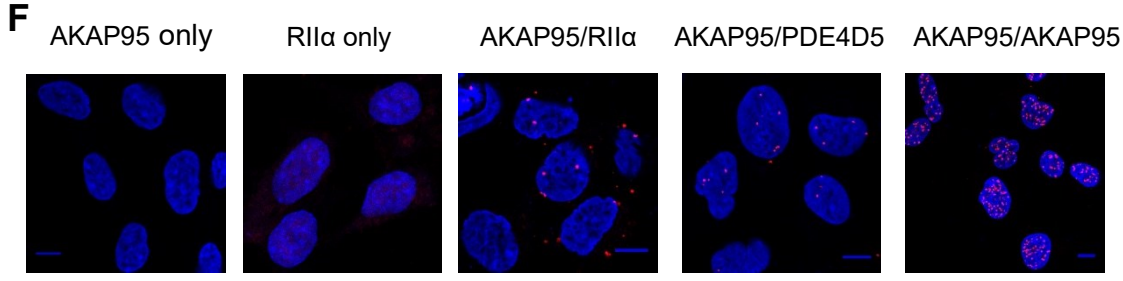

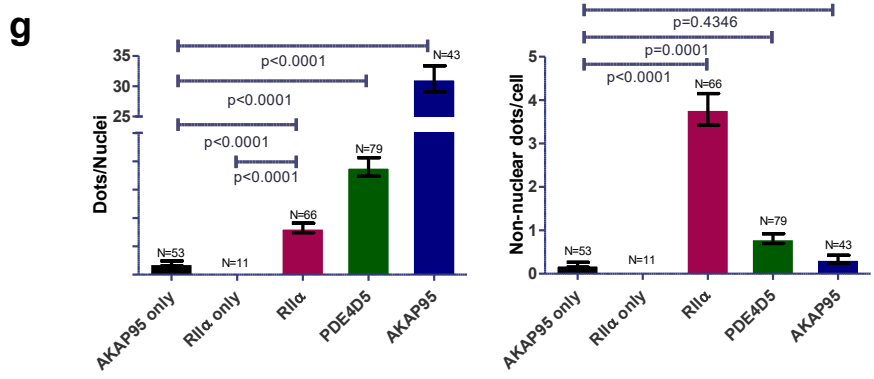

Figure S1. Related to Figure 1: Characterizing AKAP95 and its complex with PKA RIIα and PDE4D5 in the nucleus.

Fluorescence Recovery After Photobleaching (FRAP) analysis was performed to assess the mobility of AKAP95 within the nucleus. Shown here are representative cells expressing AKAP95-GFP directly before bleaching, directly after bleaching, and 5 min after bleaching. Scale bars are 10 μm. Also shown are the recovery curves indicating fluorescence in photobleached ROIs (rectangle for a and b and circle for c), both experimental (single points) and fitted (solid line). Three qualitatively different observed populations of AKAP95 were recorded, and representative cells are shown here. a) Diffuse AKAP95 readily diffuses throughout the nucleus, and has a mobile fraction on average of 65.8% (N=11 cells). b) AKAP95 puncta were also observed (white arrow). Bleaching a cross section of the nucleus that contains AKAP95 puncta shows that while AKAP95 diffuses into the bleached area, the puncta do not re-form readily. This observation is quantitatively supported by a decrease in the mobile fraction as determined by the recovery curve for this cell. c) In a separate example, AKAP95 puncta are observed in an area absent of diffuse AKAP95 (white arrow). When AKAP95 within this area of the nucleus is photobleached, it does not recover within the imaging time, suggesting that AKAP95 in that location is less mobile. d) Representative images from Figure 1 of immunofluorescence staining in HEK293T cells are shown. A rectangular crosssection of a representative cell was selected and the corresponding normalized intensity across the selection graphed. Shown is the protein of interest (PKA RIIα, or PKAcat) in green, AKAP95 in magenta, and nuclei (based on Hoescht stain) as a shaded blue area in the graph. While the nuclear signal is lower than the cytosolic signal, it is still distinctly above background. e) The difference between background (extracellular ROI) and nuclear (nuclear ROI based on Hoescht stain) signal is quantified, and for both PKAcat and RIIα there is an approximately 35-fold increase in nuclear signal over background. This difference is statistically significant ($p<0.0001$ for PKAcat and $p=0.0004$ for PKA RIIα) and supports the western blot data in Figure 1 showing the existence of these proteins in the nucleus endogenously. More detailed quantification for the PLA experiments is also shown. The data from Figure 1 are shown as well as a positive control PLA experiment using two AKAP95 antibodies. Shown are f) representative images, scale bar 10 μm, and g) a bar graph (average ± SEM) of the quantified nuclear signal (dots/nuclei). The extra-nuclear signal is also quantified and represented in a bar graph (average ± SEM). These results show that AKAP95 forms a nuclear complex with PDE4D5 and PKA RIIα in the nucleus, but that it can also form complexes in the cytosol.

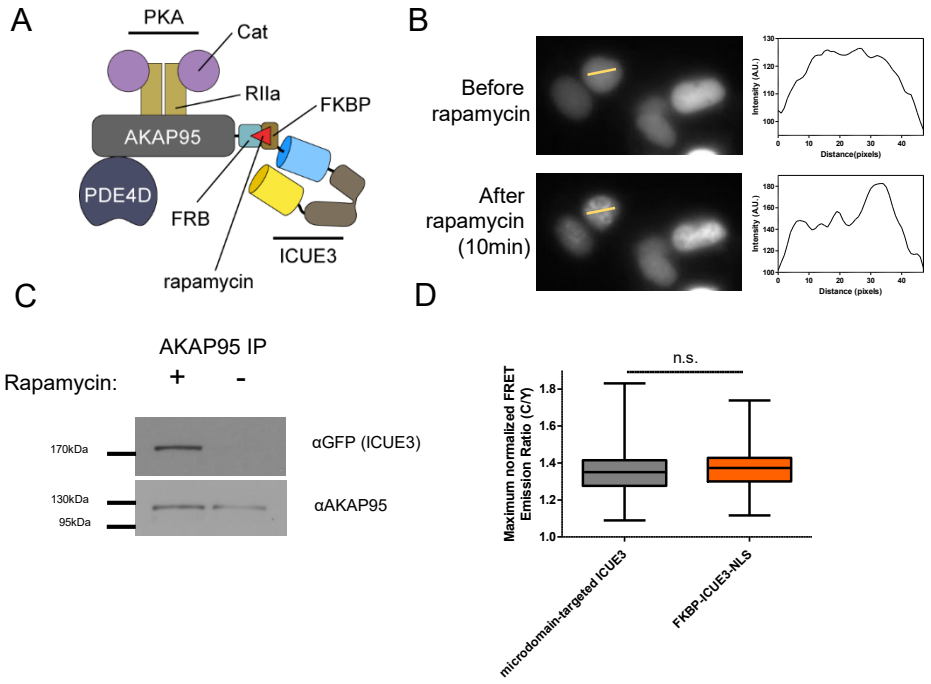

Figure S2. Related to Figure 2 and 3: Targeting ICUE3 to AKAP95

a) A schematic of targeting ICUE3 to AKAP95 is shown, repeated from Figure 2 for clarity. FKBP was fused to the N-terminus of ICUE3-NLS and FRB to the C-terminus of AKAP95. b) Upon addition of rapamycin there is a clear redistribution of ICUE3 within the nucleus, indicating that it is targeted to AKAP95. This redistribution is quantitatively shown with a line scan. c) Co-IP of HEK293T cells also demonstrates ICUE3 (detected with a GFP antibody) localization to AKAP95 in the presence of rapamycin. d) The maximum responses of ICUE3 in the nucleus or targeted to AKAP95 were compared to ensure localization to AKAP95 did not inherently limit the dynamic range of the FRET response. There is no difference ($p=0.3788$) in their response to forskolin (50 µM) and IBMX (100 µM) co-treatment (to stimulate production of cAMP and inhibit PDEs, respectively).

A

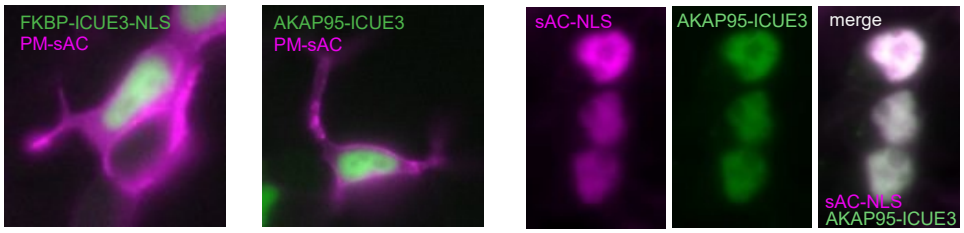

B

Individual traces and average for cells expressing PM-sAC and either FKBP-ICUE3-NLS (orange) or AKAP95-ICUE3 (black)

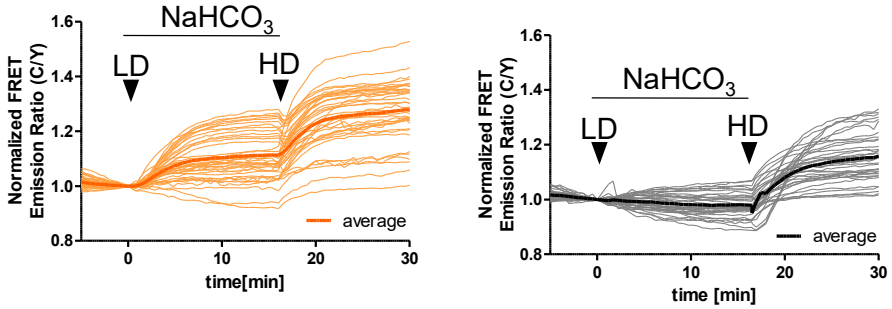

C

Individual traces and average for cells expressing AKAP95-ICUE3 and either sAC-NLS (red) or PM-sAC (black)

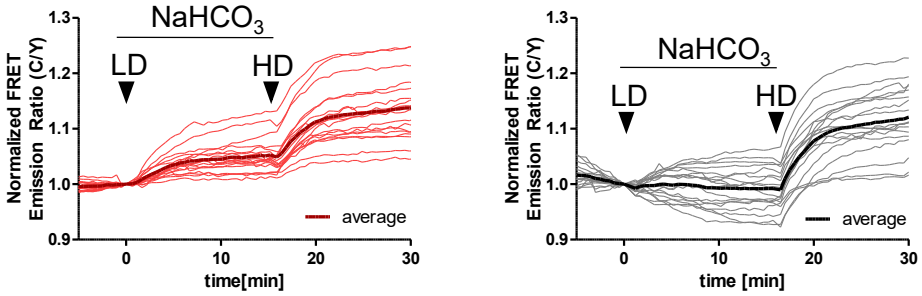

D

Individual traces and average for inhibitor pre-treatment in cells expressing AKAP95-ICUE3 and PM-sAC

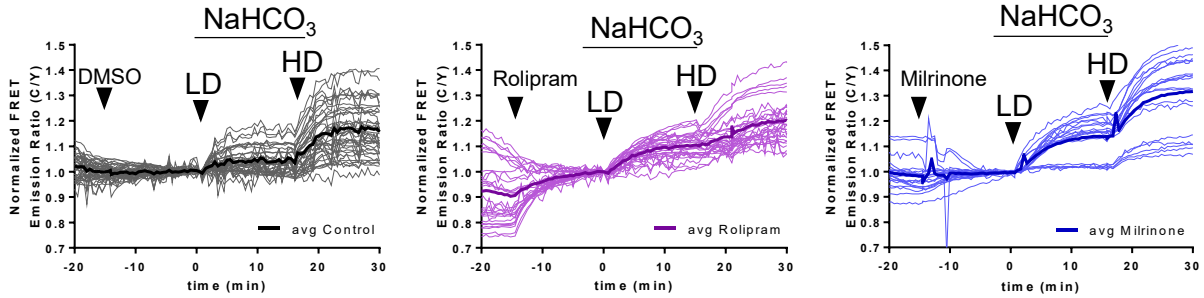

E

Individual traces and average for dnPDE4D

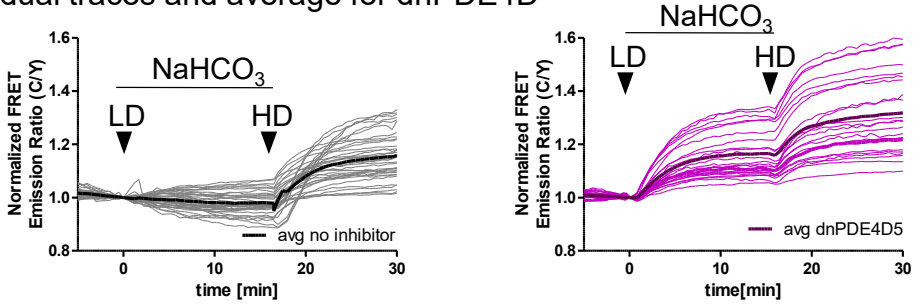

Figure S3. Related to Figure 2 and 3: Measuring cAMP around AKAP95

a) Representative images are shown to indicate localization of the biosensor and sAC in the different experimental conditions discussed in Figure 2. sAC is represented in magenta, and ICUE3 (either FKBP-ICUE3-NLS alone or AKAP95 localized ICUE3) in green. The FKBP-ICUE3-NLS samples do not express AKAP95-FRB but were still treated with rapamycin. b-e) Individual cell traces with the average (bold) are shown for the different experiments presented in Figures 2 and 3.